Journal of Computational Physics **175,** 79–107 (2002)
doi:10.1006/jcph.2001.6882, available online at http://www.idealibrary.com on IDEAL®

A Clustering Genetic Algorithm for Cylinder Drag Optimization

Michele Milano* and Petros Koumoutsakos*,†

*Institute of Computational Science, ETH Zentrum, Zürich CH-8092, Switzerland; and †CTR, NASA Ames 202A-1, Moffett Field, California 94035

Received December 12, 2000; revised June 25, 2001

A real coded genetic algorithm is implemented for the optimization of actuator parameters for cylinder drag minimization. We consider two types of idealized actuators that are allowed either to move steadily and tangentially to the cylinder surface ("belts") or to steadily blow/suck with a zero net mass constraint. The genetic algorithm we implement has the property of identifying minima basins, rather than single optimum points. The knowledge of the shape of the minimum basin enables further insights into the system properties and provides a sensitivity analysis in a fully automated way. The drag minimization problem is formulated as an optimal regulation problem. By means of the clustering property of the present genetic algorithm, a set of solutions producing drag reduction of up to 50% is identified. A comparison between the two types of actuators, based on the clustering property of the algorithm, indicates that blowing/suction actuation parameters are associated with larger tolerances when compared to optimal parameters for the belt actuators. The possibility of using a few strategically placed actuators to obtain a significant drag reduction is explored using the clustering diagnostics of this method. The optimal belt-actuator parameters obtained by optimizing the two-dimensional case is employed in three-dimensional simulations, by extending the actuators across the span of the cylinder surface. The three-dimensional controlled flow exhibits a strong two-dimensional character near the cylinder surface, resulting in significant drag reduction.

Key Words: flow control; optimization; genetic algorithm; bluff body flow.

1. INTRODUCTION

The problem of flow control has been the subject of many theoretical, experimental, and computational studies in the past few decades. Control of the flow past a circular cylinder is considered a prototypical problem of bluff body flow control.

Several methodologies for modifying vortex shedding behind a circular cylinder, either with passive geometrical modifications or with an open loop steady forcing, have been

0021-9991/02 $35.00

presented. A nonexhaustive list includes studies of the effect of a splitter plate attached to the cylinder studied, among others, by [2, 4, 26]. Properly placed holes on the surface of a hollow cylinder were also found to yield a drag reduction [27]; another possible action studied was base suction/blowing [22], and rotational oscillations were studied in [5, 24]. This latter control action was found to induce dramatic changes in the wake and a significant drag reduction.

However, the proper integration of control devices in realistic applications requires significant experimentation in order to explore the vast parameter space usually associated with the performance of these devices. Optimization techniques, such as suboptimal control [15], have been implemented in the past to identify optimal actuator configurations. These techniques require the construction of a suitable cost function and then, using the governing Navier–Stokes equations, the solution proceeds in an iterative way to provide an optimal solution to the problem over successive time intervals. Through these methods we could acquire knowledge of the controlled flow, which may lead to effective control mechanisms in practical applications. However, these methods have limited applicability to problems for which the governing equations are difficult to solve or when the design process is based on experimental and empirical settings. Moreover, these algorithms, as they require local gradient information, may converge to local minima of the optimization problem.

Stochastic optimization techniques, such as genetic algorithms (GAs) [10], circumvent some of these difficulties, as they require only the value of the cost function in terms of the control parameters. Hence they can be easily used in computational as well as in experimental studies. Moreover, they offer the capability of escaping local minima. However, there are no rigorous proofs of their convergence to global minima, which can be estimated only a posteriori. Furthermore stochastic algorithms exhibit in general a much slower convergence rate than gradient-based methods. However, this slow convergence is compensated by the inherent parallelism of the method. Information on past successes can be embedded in the optimization algorithm to further speed up the minimization process by allocating new trial points more efficiently.

An attractive aspect of genetic algorithms is that they can be adopted as an optimization "wrapper" to many flow solvers and empirical calculations. This property in conjunction with their inherent parallelism provides us with a robust optimization tool. Genetic algorithms have been applied to a number of optimization problems relevant to engineering aerodynamics, such as rotor airfoil inverse design [9], active noise control [23], high-density cooler design [21], wing shape optimization [20], optimization of diffuser blades [8], and steam turbine blades [25]. In most cases genetic algorithms have been applied to engineering problems for which there is scarce availability of other optimization techniques.

In this paper we assess the capabilities of a novel genetic algorithm as an optimization tool for the problem of flow control by studying a fundamental configuration of bluff body flows, hence allowing us to assess the validity of genetic algorithms in general in a fundamental setting. In addition to this general assessment, the capability of the algorithm proposed here of injecting physical understanding into the design process will be shown by selecting as a case study the active control of flow past a circular cylinder using as actuation the modification of the velocity on the cylinder surface. This velocity modification is achieved by two types of actuators:

(a) *ideal jet actuators*, performing a blowing/suction action on the cylinder surface, and
(b) *tangential belt actuators*, which modify the surface tangential velocity.

Mass blowing/suction actuators have been used extensively in the problem of flow control [7, 11, 13, 15]. The effect of belt actuators as a passive control device for drag reduction has been experimentally studied in [3]. A computational study of the effect of the tangential belt actuators for flow past a circular cylinder has been performed in [4]. The optimization of the actuator parameters has been developed using a number of techniques (physical insight and optimal and suboptimal control). In this article we discuss the optimization of the actuator parameters using a clustering genetic algorithm that enables the identification of sets of optimal solutions providing an automated sensitivity analysis.

In this work we consider two-dimensional flow at $Re = 500$ past a cylinder equipped with "belt" and jet actuators. Results from the optimization for the two-dimensional problem are then directly extended to three-dimensional controlled flow for the belt actuators, demonstrating significant drag reduction.

We note that the goal of this study is not only to show that it is possible to reduce the drag by using these kind of actuations but also to investigate possible correlations among the actuators. Correlations among control parameters can lead to a reduction in the number of independent inputs, thus greatly simplifying the problem. Furthermore, knowledge of the parameter sensitivity for both types of actuators can help identify which one is more suitable for the proposed application: greater parameter sensitivity implies stricter tolerance on the parameter values, which in turn usually translates to an increased difficulty in the implementation. Information on sensitivity and correlations can be valuable for a deeper understanding of the governing physical mechanisms of the controlled flow. The proposed genetic algorithm is therefore shown here to be of great help both in the desing process and in the interpretation of the results.

In Section 2 we describe the governing equations and the numerical solution to the problem. In Section 3 we present the proposed genetic algorithm. In Section 4 we discuss the results of our simulations and optimization procedure. In Section 5 some validation results for a three-dimensional simulation are presented, and in Section 6 the results obtained are summarized and some future developments are outlined.

2. GOVERNING EQUATIONS AND NUMERICAL METHOD

We consider a two-dimensional incompressible viscous flow past a circular cylinder. The governing equations are the Navier–Stokes equations

$$\frac{d\mathbf{v}}{dt} + (\mathbf{v} \cdot \nabla)\mathbf{v} = -\frac{1}{\rho}\nabla P + \nu \nabla^2 \mathbf{v} \tag{1}$$

$$\nabla \cdot \mathbf{v} = 0, \tag{2}$$

where $\mathbf{v}$ is the velocity vector, P, ρ is the pressure and density of the flow, and ν denotes the kinematic viscosity.

The boundary conditions are defined as

$$\mathbf{v}(\mathbf{x}, t) = \mathbf{V}_{ext}(\mathbf{x}_s) \quad \text{on the cylinder surface } \mathbf{x}_s \tag{3}$$

$$\mathbf{v}(\mathbf{x}, t) = U_\infty \mathbf{e}_x \qquad \text{as } |\mathbf{x}| \to \infty, \tag{4}$$

where $\mathbf{V}_{ext}(\mathbf{x}_s)$ is the externally imposed surface velocity, and $\mathbf{e}_x$ is the unit vector in the streamwise direction. The Reynolds number and Strouhal frequency of the flow are

normalized quantities defiend as

$$Re = \frac{U_\infty D}{\nu} \quad St = \frac{f\,D}{U_\infty},$$

where $D = 2R$ is the diameter of the cylinder and f the shedding frequency of the flow.

The equations are discretized using a staggered, second-order central-difference method in generalized coordinates [17]. The solution is advanced in time using a fractional step scheme, in which a third-order Runge–Kutta scheme is used for the nonlinear convection terms and a Crank–Nicholson scheme is used for the viscous terms. A multigrid solver is used in conjunction with a Gauss–Seidel line-zebra scheme to solve the pressure Poisson equation.

An O mesh has been used in this paper. The size of the computational domain has been set to 30 cylinder diameters, as proposed by benchmark tests in [18].

Simulations were carried out to find the coarsest mesh yielding reliable results, to minimize the simulation time needed for one fitness function evaluation. Three uncontrolled flow simulations were carried out using meshes of different resolutions, $N_r \times N_\theta = 40 \times 80$, 80×160, and 160×320, while the time step was fixed to 0.003 for all cases. The drag and lift coefficients resulting from the different simulations are compared in Fig. 1. The results for all three resolutions are in reasonable agreement so that the coarsest mesh was used in the optimization process. To confirm the validity of the optimization parameters, at the end of each optimization cycle a validation run was performed on the finer $N_r \times N_\theta = 80 \times 160$ mesh. The change in the average drag coefficient and the rms value

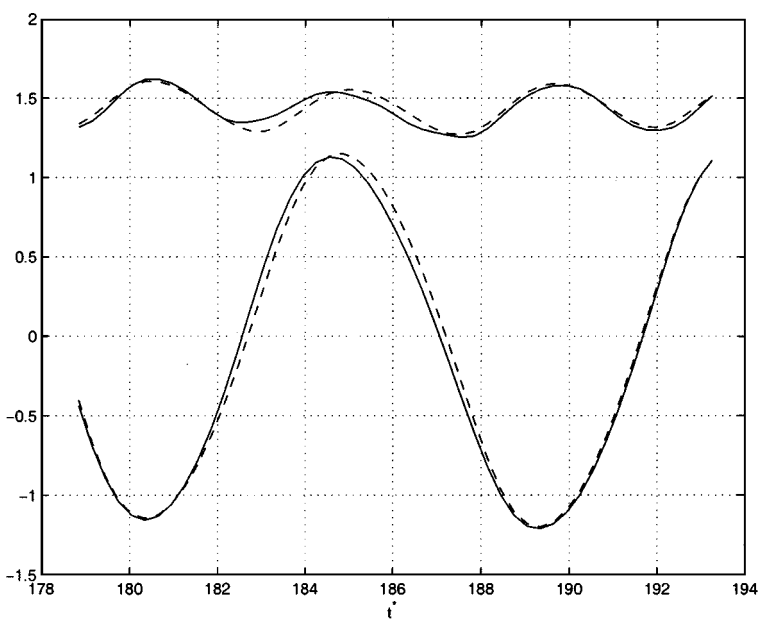

FIG. 1. Drag coefficient C_D (upper curves) and lift coefficient C_L for simulations using different meshes. Dashed: 80×160 mesh, solid: 40×80 mesh (all $N_r \times N_\theta$). The 160×320 mesh results are not shown, since they coincide with the 80×160 mesh results.

in the higher resolution calculation was within 10% of the coarse mesh calculation and the results reported in this work are those from the refined validation runs.

3. PROBLEM SETUP

We consider first the two-dimensional incompressible flow at $Re = 500$ past a circular cylinder. The cylinder surface is subdivided in $n = 16$ equally sized segments (Fig. 2). Two different control actions are considered:

(i) Each segment is allowed to move tangentially to the cylinder surface, with all the segments moving with different but steady velocities.

(ii) Each of the segments is considered to be an ideal mass transpiration actuator, with a zero net mass flow imposed as a constraint in this case.

As discussed in the following sections, of particular interest is the capability of the GA used herein to automatically identify critical points such as the separation points of the uncontrolled flow. For $Re = 500$ these points are encompassed by actuators 4 and 13 on the cylinder surface.

The drag coefficient of the flow is defined as

$$C_D(\omega) = \frac{2}{\rho U_\infty^2 D} \int_{cyl} (p(\omega)\mathbf{n}_\mathrm{x} - \tau_{\mathrm{ix}}(\omega)\mathbf{n}_\mathrm{i})\, dl, \tag{5}$$

where p is the pressure and τ_{ix} the viscous stress tensor on the surface of the cylinder; $\omega = \{\omega_1, \ldots, \omega_\mathrm{n}\}$ is a vector of $n = 16$ components representing the actuation strengths of the surface actuators. This equation, together with Eqs. (1)–(4), defines the model of the system to be controlled. The input of the system is the surface velocity, which can be manipulated by means of tangential belts or ideal jet actuators; the output is the drag coefficient.

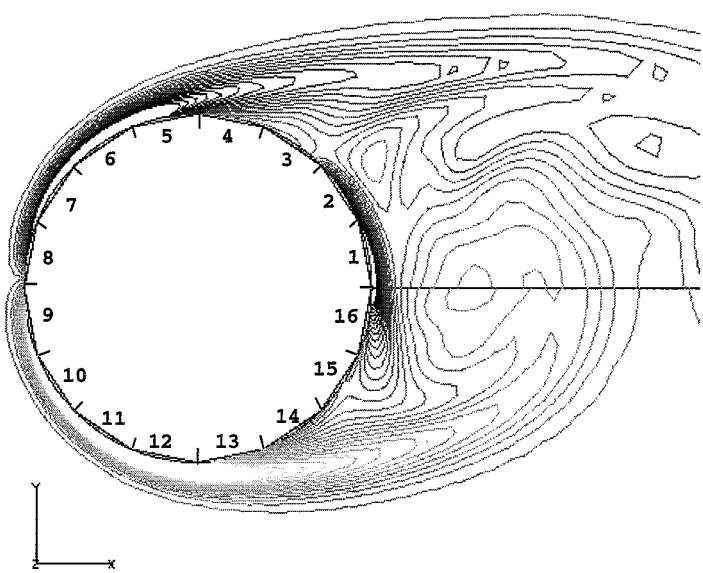

FIG. 2. Position of the actuators on the cylinder surface. Snapshot of the uncontrolled flow vorticity.

An optimal regulation problem [1] can be set up by considering the functional

$$J(\omega) = \sqrt{\frac{1}{H}\int_0^H \left[C_D^2(\omega) + \omega^T R\omega\right] dt}, \tag{6}$$

where ω is the input vector, H is the time horizon considered, which in the present case will be four times the Strouhal period of the uncontrolled flow, and R is the input weighting matrix. The functional 6, subjected to the constraints 1, 2, must be minimized with respect to ω in order to minimize the drag.

We note here that the uncontrolled flow at $Re = 500$ is three-dimensional. However, our goal is to examine a control strategy for the two-dimensional flow. The results of this control strategy are then implemented in a three-dimensional setting.

4. THE OPTIMIZATION ALGORITHM

The genetic algorithm used in this paper operates on a parameter population in which an input vector ω consists of *one population member*. Three operators are defined to modify the population members:

- *Recombination/crossover*, which generates new trial solution points (offsprings), using some elements drawn from the population.
- *Mutation*, which randomly changes some of the offsprings' components.
- *Selection*, which chooses the population elements that will be used by the crossover.

For each population element a *fitness function* is defined, measuring in a quantitative way how close a given solution is to the desired goal. Based on their fitness, the old population members are compared with the newly generated ones, and the solutions with the better fitness constitute the new population members. In this way, iterating the selection–crossover–mutation process, the population evolves toward the desired optimal solution.

The optimization algorithm used in this paper is a real coded GA that is particularly suitable for finding clusters of good solutions [16], a desirable scheme when smooth, nonsingle point minima are sought. A variable mutation operator, depending on the local fitness value and on the global success history of the population, allows the population to avoid local minima.

In a first phase S population points are initially randomly chosen according to a uniform distribution within a defined search volume of dimension n. Let the function to be minimized be denoted by $J(\omega)$. The inequality $S \gg n$ must hold for the algorithm to properly work. After the end of this first phase, the algorithm proceeds as follows:

Step 1: Choose the grid point ω_{max} in which J reaches the maximum value:

$$\omega_{max} = \arg\left[\max_{i=1,\ldots,S} J(\omega_i)\right]; \quad J_{max} = J(\omega_{max});$$

Step 2: Choose $n+1$ different grid points at random: $\omega_1, \ldots, \omega_{n+1}$ (breeding set). All the subsequent operations are performed on this set;

Step 3: *Mutation step*: for all the breeding set points, with probability

$$P_i = (1-\alpha^I) \cdot \left(1 - \beta^{\frac{(J(w_i)-J_T)}{J_{\alpha v}}}\right) \cdot \gamma, \tag{7}$$

replace the point ω_i with a completely random point, chosen within the search volume limits;

Step 4: *Recombination step*: for each of the $n+1$ points determine the centroid, $\underline{\omega_i}$, of the other n points; i.e.,

$$\underline{\omega_i} = \frac{1}{n} \sum_{j=1,\, j\neq i}^{n+1} \omega_j . \tag{8}$$

(a) Generate the offspring $\omega_{si} = 2\underline{\omega_i} - \omega_{n+1}$; if ω_{si} is not contained in the search volume, process next point in the breeding set;

(b) Calculate $J(\omega_{si})$; if $J(\omega_{si}) < J_{max}$ then ω_{max} is purged from the population and is substituted by the offspring ω_{si};

Step 5: *Selection step*: Compute the new J_{max}, if necessary;

Step 6: Iterate steps 4 and 5 on the whole breeding set;

Step 7: If the convergence test is not satisfied, return to step 1.

This GA is characterized by four parameters, α, β, γ, J_T, and two variables, I and J_{av}, which are defined in this scheme.

The variable I is the number of consecutive iterations in which the population has not been changing; i.e., no offspring substituted any population member. It gives an empirical measure of the necessity of introducing some new information in the population, by increasing the mutation probability. The variable J_{av} is the average value of the population fitness: it is used as a scaling factor.

The parameter J_T is a threshold value for $J(\omega)$ used for the convergence test: if all the population fitness values are smaller than this threshold, then the convergence is declared. With this convergence criterion, the population points will be clustered inside the domain defined as $w : J(\omega) < J_T$. This final cluster can provide useful information about correlations among the parameters as well as information regarding the sensitivity of the cost function to these parameters.

The parameter $0 \leq \alpha \leq 1$ modulates the mutation rate during the optimization process, and the parameter $0 \leq \gamma \leq 1$ enforces an upper bound to the mutation probability, since $0 \leq \beta \leq 1$. The term containing the parameter β modulates an order relationship between the population members. Namely, members that are further away from the target have a greater mutation probability due to this term.

These parameters are inherent to the present optimization scheme. They may be viewed as modeling coefficients that aid the algorithm to identify its environment, which, when suitably selected, can increase the rate of convergence of the scheme. In convergence studies of the algorithm [16] for multidimensional prototypical cost functions these parameters were in turn allowed to vary to optimize the overall convergence rate of the scheme. Their optimal values were found to be not so critical in this study. More specifically, the parameters α and β have been found to have no significant influence on the convergence properties of the GA when varied within the range of [0.1, 0.9], while the upper bound γ resulted in playing a more important role in escaping local minima; an empirical rule for setting this upper bound can be to initially set it to the inverse of the population size, i.e., $\gamma = 1/S$, so that the maximum mutation probability for a population member equals the probability of choosing at random one population member. If the desired goal is not reached and the GA appears stuck in a local minimum, then γ can be increased, thus increasing the exploration capabilities of the GA.

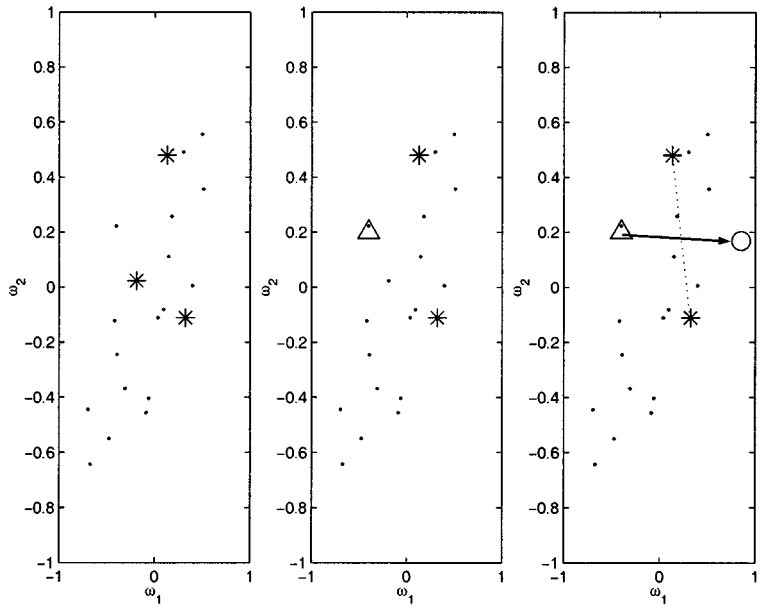

FIG. 3. Illustration of the mutation/recombination mechanism, for a 2D parameter space. Left: Population (dots) and breeding set (∗); center: mutation of one breeding set point (triangle); right: generation of a new offspring (circle).

However, no precise setting rule was identified and the parameter selection remains a part of an ad hoc design depending on the fitness function, for this optimization algorithm. Work is under way to make these values online adaptive using information obtained during the optimization process and adopting biologically inspired models of population behavior. To illustrate the core mechanisms of the algorithm, a sketch demonstrating the recombination and mutation mechanisms is shown in Fig. 3 for a function of two parameters.

As a further example of the operation of this GA, the following test function of two parameters is considered here:

$$J_{test}(\omega_1, \omega_2) = 74 + 1000 \cdot \left(\omega_2 - \omega_1^2\right)^2 + (1 - \omega_1)^2 + -400 \cdot e^{-\frac{(\omega_1+1)^2+(\omega_2+1)^2}{0.1}}, \quad \omega_1, \omega_2 \in [-2, 2]. \tag{9}$$

The test function has a local minimum near (1, 1), with a quite large banana-shaped basin, and the global minimum is near $(-0.91, -0.94)$; $J_{test}(1, 1) = 74$, $J_{test}(-0.91, -0.94) = 34.43$. The global minimum is sharper than the local minimum, with a smaller basin. Figure 4 shows different instances of the population during the minimization process, together with a contour plot of the function.

A population of $S = 50$ elements is used for this minimization task, with the parameters $(\alpha, \beta, \gamma) = (0.25, 0.25, 0.02)$. The threshold J_T has been fixed to 60. The population is fairly uniformly distributed inside both basins after a small number of iterations, thus optimizing the allocation of new trial points; the correct minimum basin is correctly identified after further exploration of the search volume has taken place, and when the worst

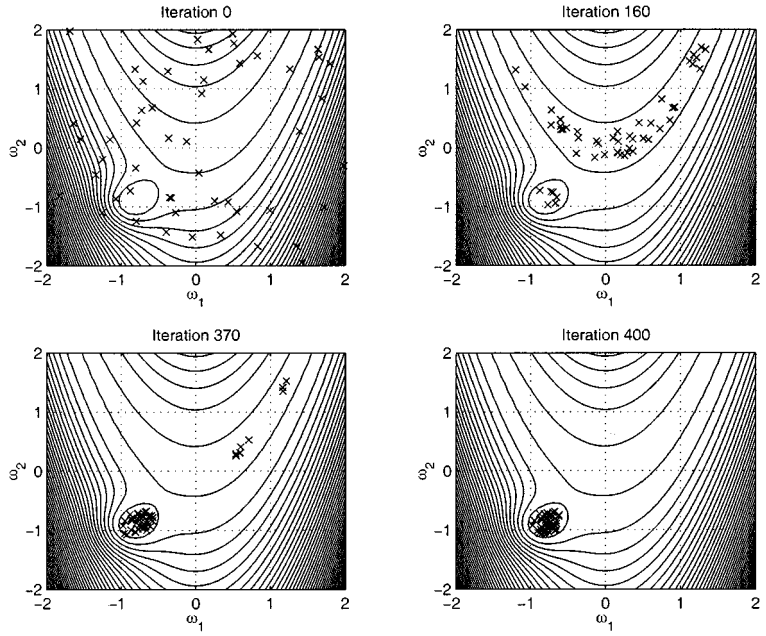

FIG. 4. Minimization of the modified Rosenbrock function. Level curves of the function: The closed curve centered on $(-1, -1)$ contains the global minimum basin; the banana-shaped basin contains a local minimum located in (1, 1). The population is denoted by "x" symbols. Some snapshots of the population during the minimization process are shown.

population member fitness becomes smaller than J_T, convergence is declared. The final population satisfactorily approximates the global minimum basin.

5. RESULTS

We present here the results of the optimization algorithm for cases in which no penalty terms are introduced for the control energy, i.e., $R = 0$ in Eq. (6), and for cases in which the penalizing term is introduced. Note that without any penalization for the control energy it is possible to derive an upper bound for the regulator performances and also to obtain physical insight into the system behavior. In this context it will be shown how the optimized population cluster automatically identifies the actuators that are the most influential for achieving drag reduction.

In the next sections the following cases will be considered:

5.1. No penalty terms, belt actuators
  5.1.1. Control using all the actuators
  5.1.2. Control using the most influential actuators
5.2. No penalty terms, mass transpiration actuators
  5.2.1. Control using all the actuators
  5.2.2. Control using the most influential actuators
5.3. Penalty terms
  5.3.1. All the actuators, belt actuators
  5.3.2. All the actuators, mass transpiration actuators
5.4. Control of three-dimensional flow with belt actuators

5.1. No Penalty Terms, Belt Actuators

Here we distinguish between results obtained with all 16 actuators of the cylinder surface active and a subsequent case where the active actuators are those exhibiting high correlation in the first case.

5.1.1. *Control Using All the Actuators*

A population of $S = 50$ elements was chosen for the GA; the parameters α and β were fixed to 0.25; this setting for these two parameters is the same as that in [16]. The upper bound γ has been set to $1/S = 0.02$, as discussed in Section 4.

The threshold J_T was fixed to 0.8; this threshold value corresponds to an average drag coefficient that is 50% of the drag coefficient of the uncontrolled flow at $Re = 500$ [19].

In Fig. 5 the worst fitness value in the population as a function of the iterations performed is reported; the algorithm converged after about 260 iterations. One GA iteration corresponds to the evaluation of the fitness function on 17 offsprings; therefore the number of function evaluations can be obtained by multiplying by 17 the number of iterations. However, in this paper we implemented a parallel version of the GA, by simply performing the offsprings' computations in parallel on 17 different processors. We used a Cray J90, on which the entire optimization process took about 4 h of CPU time.

To investigate the final population, in Fig. 6 a histogram of the distribution of the population cluster is reported. It can be observed that most parameters are not clustered, an indication of the fact that they have little influence on the fitness function. The most evident clustering can be observed for the velocities assigned to actuators 3–4 and 13–14, which contain the separation point of the uncontrolled cylinder.

The solution yielded by the GA indicates that these actuators (3–4 and 13–14) on opposite sides of the cylinder must always rotate in opposite directions, to delay separation by

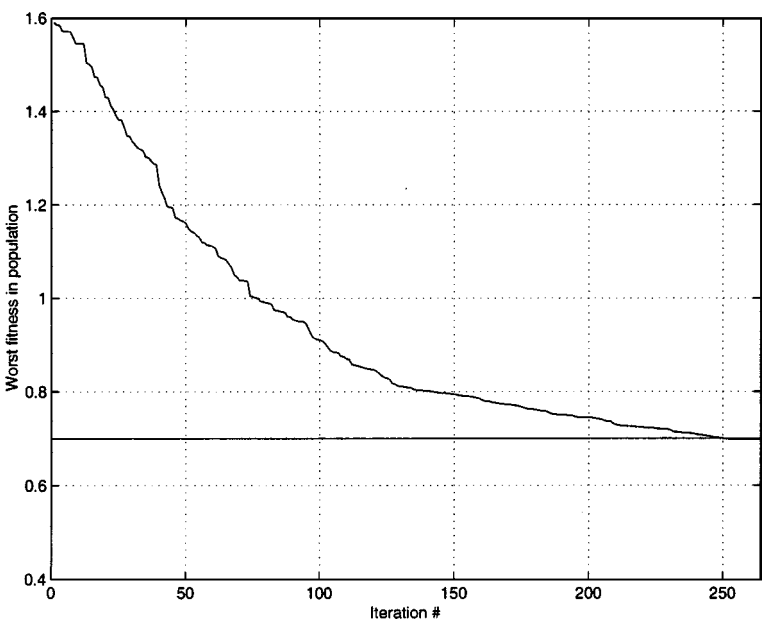

FIG. 5. Worst fitness squared in the population as a function of the optimization process iterations. The horizontal line is the desired target value.

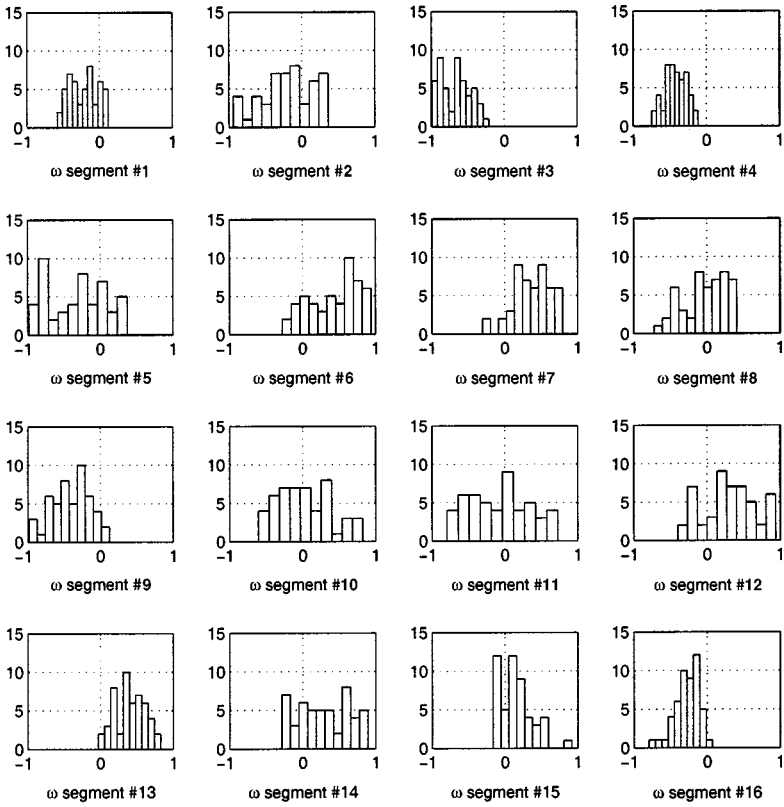

FIG. 6. Histogram of the population cluster.

allowing the flow to "slide" more on the cylinder surface. A closer look at the velocity of actuators 4 and 13 reveals no significant correlation between them (Fig. 7). This suggests that the relevant feature for drag reduction is only the direction of motion of the actuators and that it must be in opposite directions at all times for the present configuration. No significant correlations were found between all the other parameters.

To provide a quantitative measure of the parameter clustering, we normalized parameter mean values in the population with the corresponding standard deviations. This quantity is similar to the z score of a distribution [28], defined as

$$z_x = \frac{x - \mu_x}{\sigma_x}, \tag{10}$$

where x is an element of the distribution and μ_x, σ_x are the distribution's mean and standard deviation, respectively. In our case we needed a quantity that measured how much a distribution is clustered away from zero; therefore we define a "z score of the mean with respect to zero" for each segment

$$z_i = \frac{|\mu_i|}{\sigma_i}, \quad i = 1, \ldots, 16, \tag{11}$$

where μ_i, σ_i are the mean value and standard deviation of the velocities for the segment i, respectively. A value $z_i = 0$ holds for a distribution that is perfectly centered around zero,

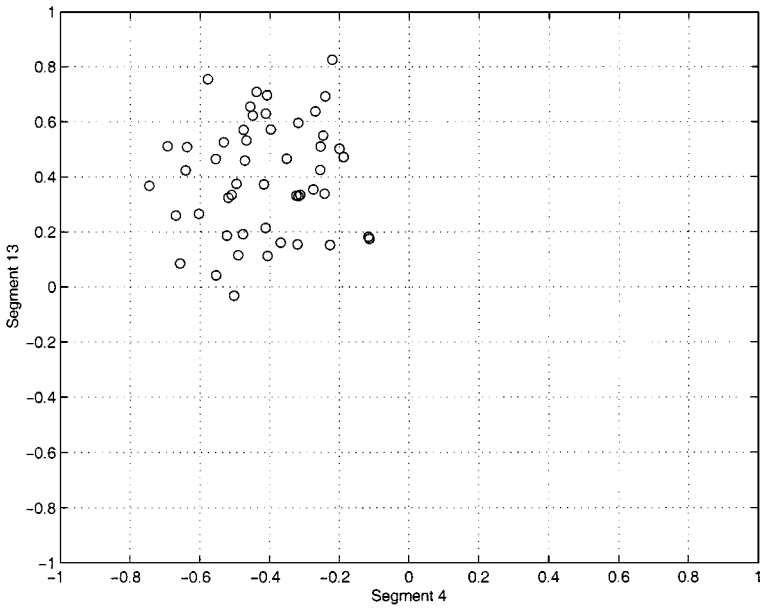

FIG. 7. A plot of the angular velocity ω for the actuator 4 vs ω for the actuator 13. No evident correlation can be appreciated, apart from the difference in the sign.

while larger values for z_i denote distributions that are more clustered at greater distance from zero, as desired.

The antisymmetric actuation found for the segments containing the separation points suggests that the significance of the solutions should be analyzed for pairs of actuators that are symmetric with respect to the horizontal diameter. For this purpose we define a "joint z" for pairs of actuators

$$zj_i = \frac{|\mu_i|}{\sigma_i} + \frac{|\mu_{17-i}|}{\sigma_{17-i}}, \quad i = 1, \ldots, 8, \tag{12}$$

where the index i denotes pairs of symmetric actuators, ranging from $i = 1$ (actuators 1 and 16) to $i = 8$ (actuators 8 and 9). The pairs of actuators containing the separation points are the pair numbers 3 and 4. This quantity measures how many pairs of symmetric actuators are clustered away from zero by summing the absolute values of the means normalized by the respective standard deviations. Also in this case, larger values of zj_i denote more significant clustering.

In Fig. 8 the joint z score defined here is reported for all the pairs of symmetric actuators. It is possible to see that pairs 3 and 4 clearly yield the highest joint z score, thus confirming also quantitatively our conclusions.

In Fig. 9 the behavior of the separation points is shown for the controlled cylinder; after the transient phase there is a marked increase of separation/reattachment events, indicating the formation of many recirculation bubbles streamlining the flow along the cylinder. This serves as evidence that the GA is able to identify the critical points of the flow and to communicate them via the clustering of its population members.

To examine further the optimized configuration, a validation run was performed for the best solution in the population. This run was performed on a finer grid, as specified earlier.

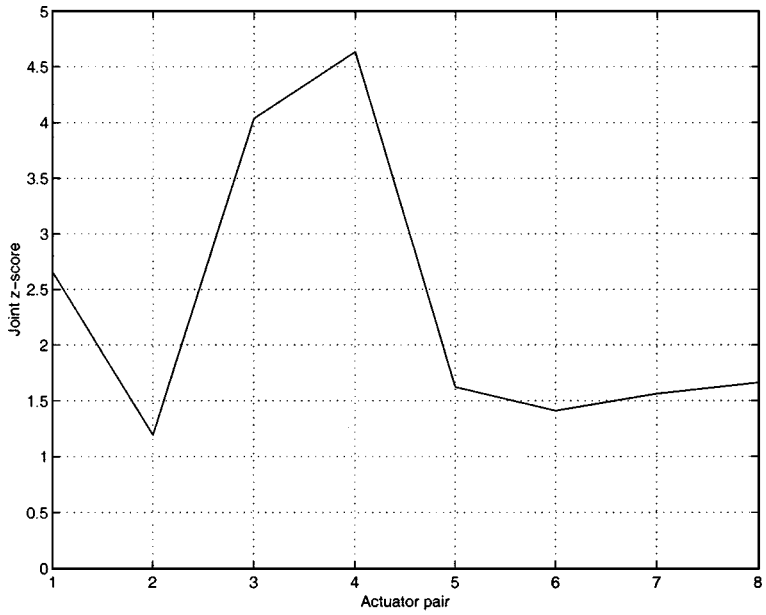

FIG. 8. Joint z scores for pairs of symmetric segments. See text for the definition of this quantity.

In Fig. 10 the behavior of the drag coefficient during the transition from the uncontrolled and controlled phase can be observed. The transition phase is quite short, and the flow appears to settle quickly to the minimal drag configuration. The shedding frequency is drastically modified, while the fluctuating amplitude in the drag coefficient is drastically reduced.

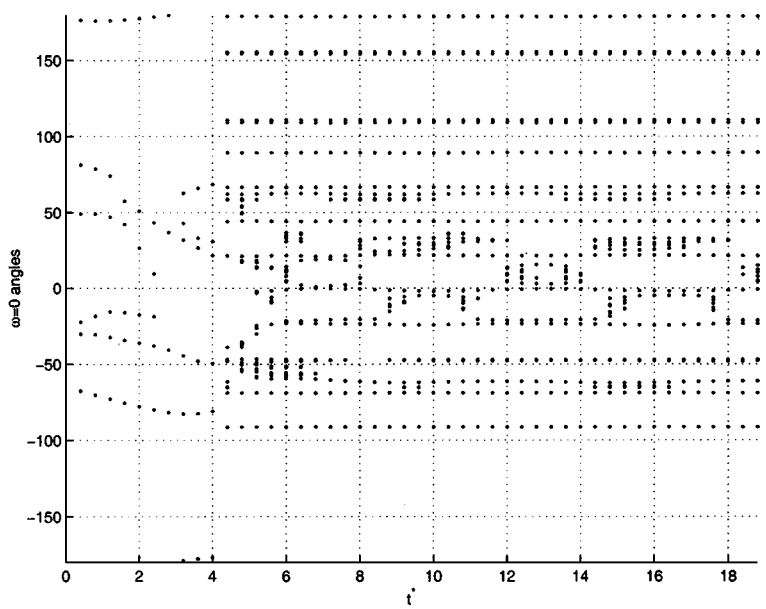

FIG. 9. Positions of the separation/reattachment points along the cylinder surface. Angles are measured between -360 and $+360$ degrees, w.r.t. the center axis of the wake.

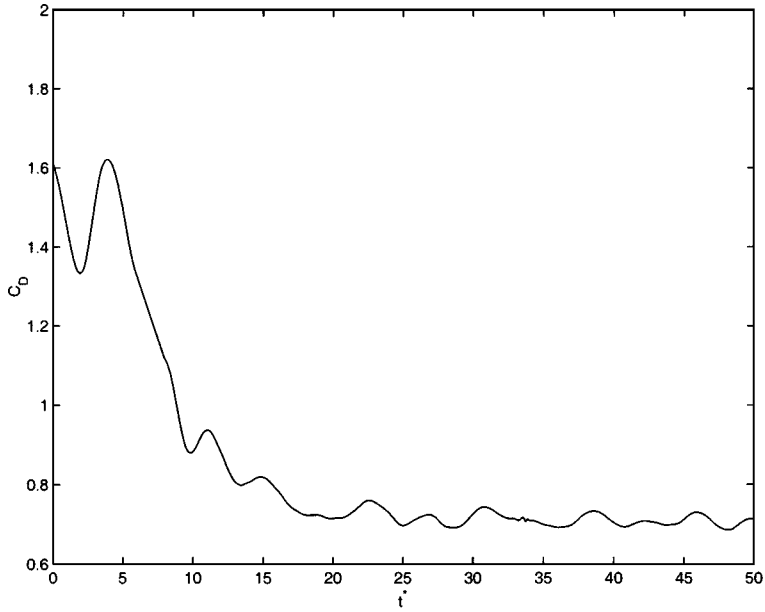

FIG. 10. Validation run for the best population member. The control is switched on at $t^* = 5$.

In Figs. 11 and 12 time averages of the vorticity contours in the near wake region are shown. They reveal that the wake becomes very elongated, evidence that the vortices begin to detach and roll up at larger distances than in the uncontrolled case, thus reducing the loss of pressure in the back side of the cylinder. It is evident that the flow stays attached for longer on the surface while a well-defined recirculation bubble is formed, thus streamlining further the effective shape of the body.

Snapshots of the vorticity contours in the near wake region are shown in Fig. 13 for the uncontrolled case, for the transition from the uncontrolled to the controlled phase, and

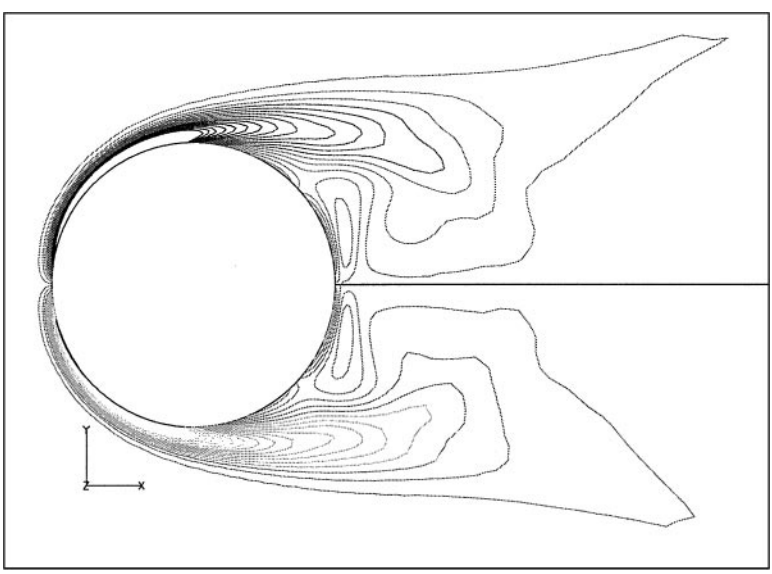

FIG. 11. Time average of the vorticity contours near the cylinder, no control.

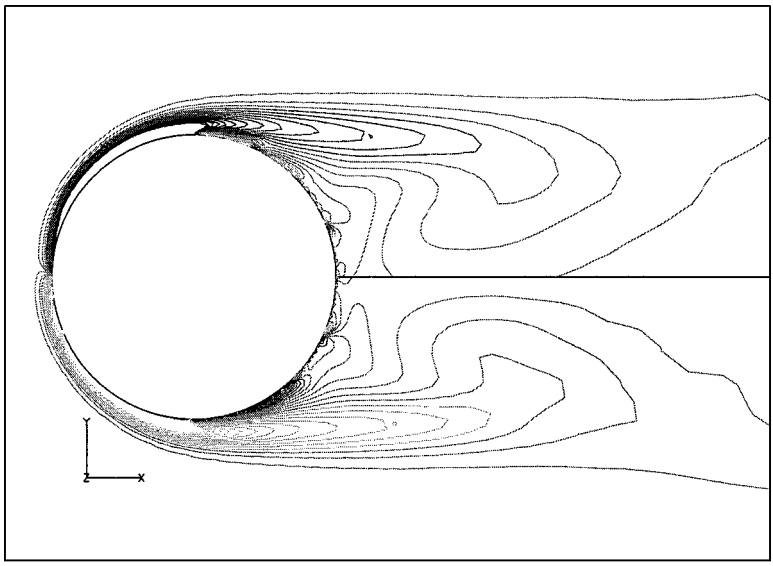

FIG. 12. All the actuators active: Time average of the vorticity contours near the cylinder, control switched on.

during half a period of the controlled phase. The wake elongation phase and the change in the vortex shedding are clearly visible from these plots.

Turning the attention to the GA population cluster, apart from actuators 3– 4 and 13–14, the parameter clustering has no evident symmetry around the streamwise direction. The lack of symmetry in the control action can be attributed to the fact that most of the actuators have little influence on the drag reduction, since the corresponding parameters are not clustered.

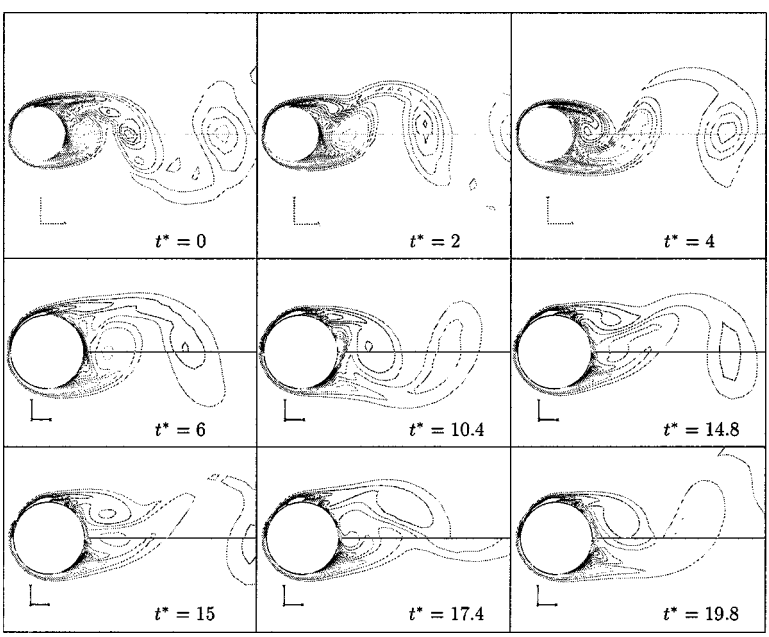

FIG. 13. Snapshots of the vorticity contours near the cylinder. Top row: Uncontrolled half Strouhal period; middle row: transition to the controlled mode; bottom row: controlled mode.

TABLE I
Results Found by the Clustering GA for Different Search Volume Limits

Limits	Drag reduction
$[-0.01, 0.01]$	$<1\%$
$[-0.1, 0.1]$	40%
$[-0.5, 0.5]$	45%
$[-1, 1]$	50%

Hence it appears natural to suggest that the important parameters for the flow control are only the ones corresponding to actuators containing the separation point in the uncontrolled flow. At the same time all the other actuators could be sliding with random velocities or remain fixed. To verify this hypothesis another validation run was performed, this time maintaining active only actuators 3–4 and 13–14. In Fig. 14 the time-averaged vorticity contours are shown. This plot shows that also in this case the wake elongates almost as before.

Optimization runs were performed in search volumes with different limits for the actuator velocities, in order to check the optimal control performances for different optimization limits. Table I reports the optimization results for four different search volume limits.

The limit for the actuator amplitude under which it was not possible to achieve a significant reduction with this type of actuation is 0.01. With this amplitude limit the population

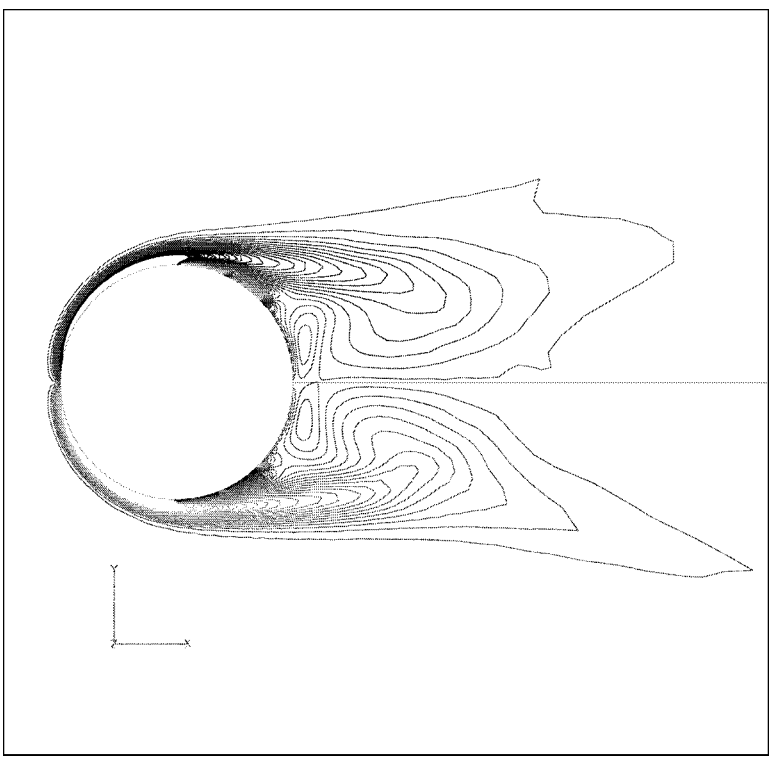

FIG. 14. Only four actuators active: Time-averaged vorticity contours near the cylinder, control switched on.

parameters showed no significant clustering. For all other limits the population clustering was the same as that for the limits of $[-1, 1]$.

5.1.2. *Optimization of the Most Influential Actuators*

To analyze the effects of the four actuators exhibiting clustering and thus being considered of fundamental influence on the drag reduction mechanism, another optimization run was performed using only these four actuators as free parameters. Here it should be emphasized that no a priori knowledge of the separation points was necessary as the algorithm was able to identify them through the parameter clustering.

In this case a population of 20 elements was used for actuators 3, 4, 13, and 14, with all the other actuator parameters set to zero, in order to study the effect of these actuators in detail. The threshold J_T was set to 0.86, which is the value attained for the fitness function using only four parameters.

The population clustering in this case is shown in Fig. 15. Comparing these histograms with those shown in Fig. 6, it is possible to see that the symmetry is lost in this case as the values for ω_3 are closer to 0. In the case of the optimization with all the actuators available, the values of ω_3 are closer to 0.5, and the same is true for ω_4; on the other hand, for the four parameters the optimal magnitude of ω_4 is larger with respect to the other case. The other two parameters are much better clustered than in the earlier case, indicating that using less degrees of freedom the parameter sensitivity increases. The z-score analysis is not necessary in this case, since the clustering is clearer than before.

In this case some correlation was found between the parameters ω_4 and ω_{14}, shown in Fig. 16. No other significant correlation was found. Contours of the near wake vorticity do not exhibit any marked difference from those shown in Fig. 14.

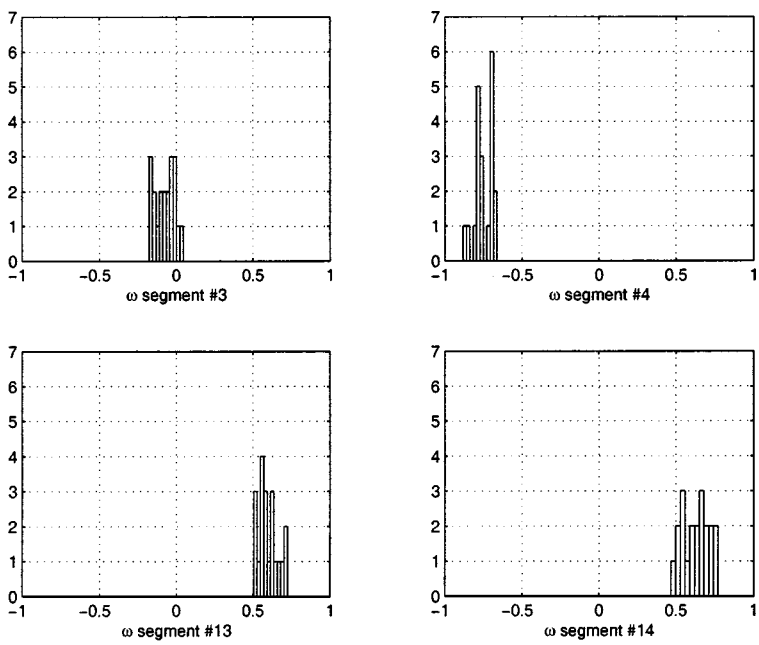

FIG. 15. Optimization with only four actuators. Histogram of the population cluster.

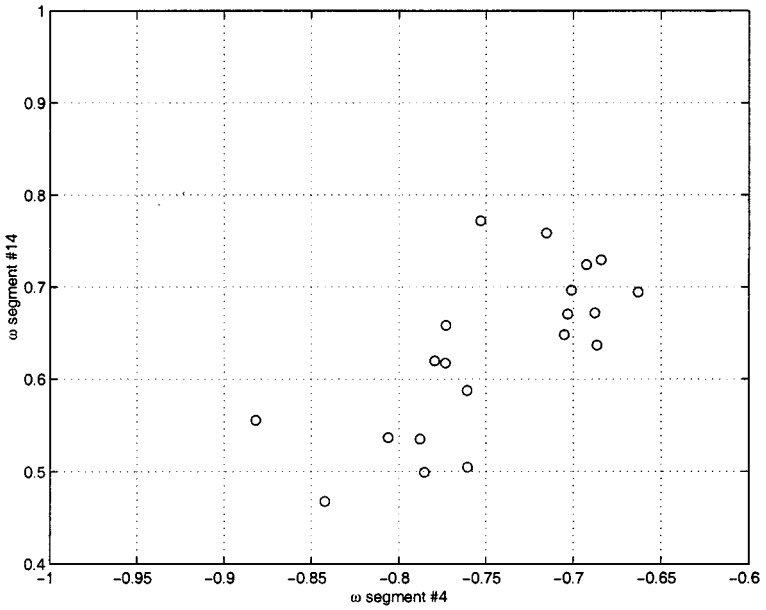

FIG. 16. Optimization with only four actuators. A plot of the parameters showing a significant correlation.

However, as can be noted from the comparison between the drag coefficients for the two control configurations, reported in Fig. 17, the drag reduction in the present case is smaller w.r.t. the reduction given by using all the 16 belt actuators.

Hence these results demonstrate that in this case a larger drag reduction is feasible by allowing more degrees of freedom to the actuator parameters. By actuating beyond the

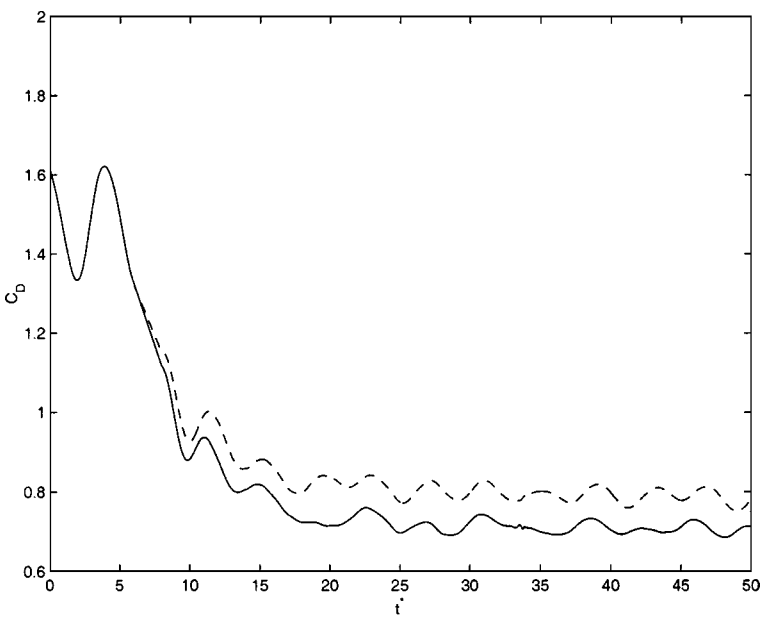

FIG. 17. Comparison between the drag coefficients for the two cases using the belt actuators. Continuous line: all the actuators, dashed line: only the most influential actuators used.

vicinity of the separation points it is possible to adjust the flow velocity before it arrives at the separation point so that the actuators in that region do not face an abrupt change of the environment that they are attempting to control. The absence of any correlation in the rest of the actuators suggests that it would be difficult to identify an a priori estimate of the actuator profile for large numbers of actuators, even for this simplified geometrical configuration.

5.2. No Penalty Terms, Mass Transpiration Actuators

The same set of experiments as before is presented here. Also in this case the separation point of the uncontrolled flow has been identified by the GA to play a critical role in the drag reduction mechanism, so we maintain the distinction between results obtained with all 16 actuators active and results where the active actuators are those exhibiting high population correlation in the first case.

The results obtained with these kinds of actuators are very similar to those obtained with belt actuators; some of these results are reported in what follows.

5.2.1. *Results Using All the Actuators*

In the case of blowing/suction actuation, all the GA parameters including the threshold J_T were kept equal to the case of the tangential actuation, in order to consistently compare the optimization performance of the two types of actuators.

In this case the GA did not converge to the desired threshold, and the limit of 1000 iterations was reached without significant improvements of the worst fitness; the mutation probability was saturated to its maximum allowed value, as is clear from Fig. 18. This is evidence that there is a high probability that the minimum reached is a global one.

A histogram of the final population cluster is shown in Fig. 19. Also in this case most parameters are not clustered, and the most evident clustering can be observed for the velocities assigned to actuators 3–4 and 13–14, also for these kinds of actuators. This means

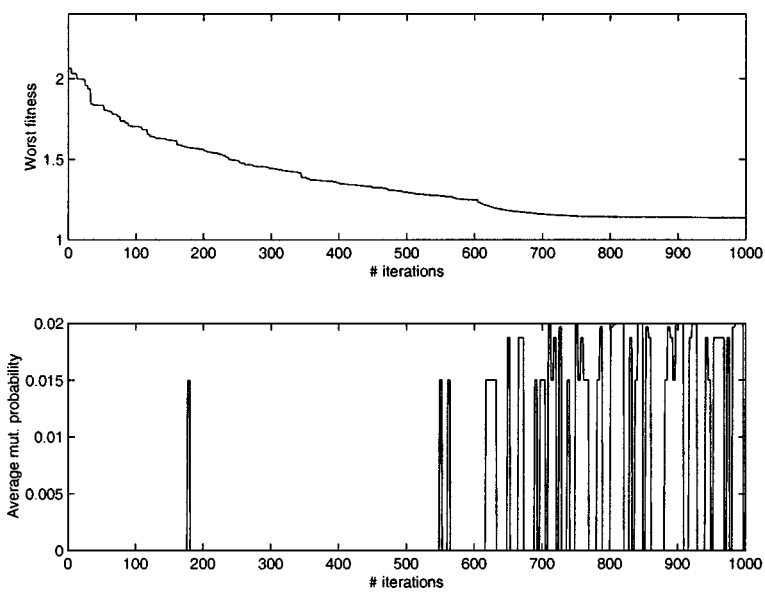

FIG. 18. Ideal jet actuators. Top: Worst fitness in the population as a function of the optimization process iterations; bottom: mutation probability averaged over the population.

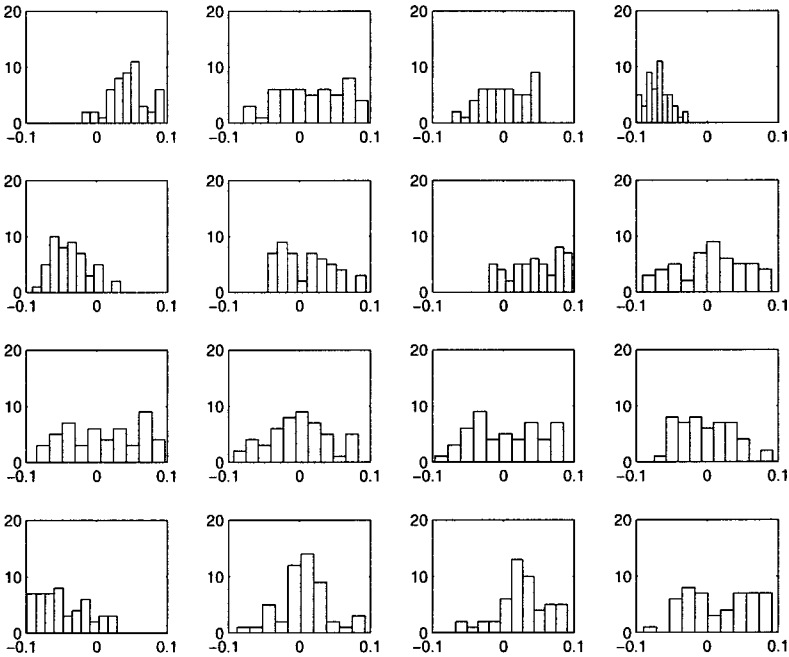

FIG. 19. Population clustering, ideal jet actuators: All the parameters are active.

that these actuators are the most important also in this case; however, the solution yielded by the GA indicates that these actuators (3–4 and 13–14) must always operate on a suction mode, to delay separation by allowing the flow to "slide" more on the cylinder surface.

Also in this case the most important segments for control are those containing the separation point, as indicated by the joint z scores reported in Fig. 20.

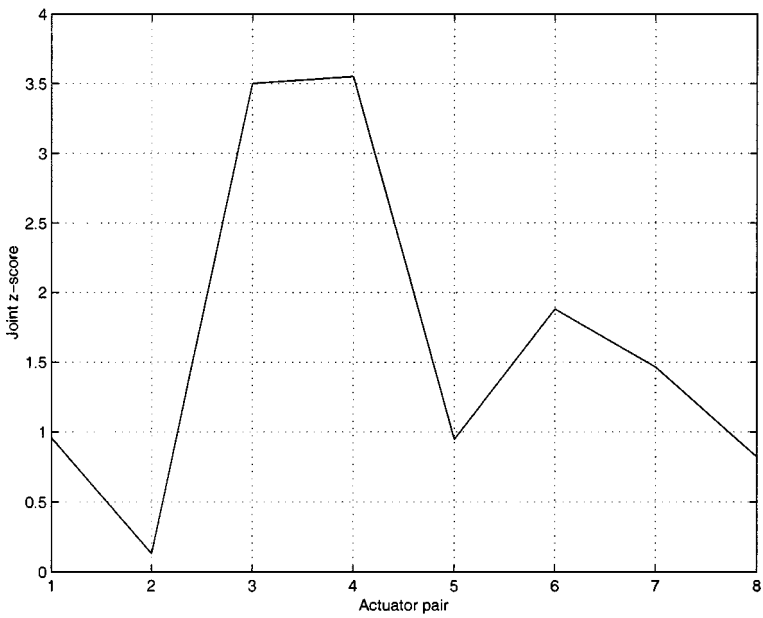

FIG. 20. Jet actuators, joint z scores for the optimized population.

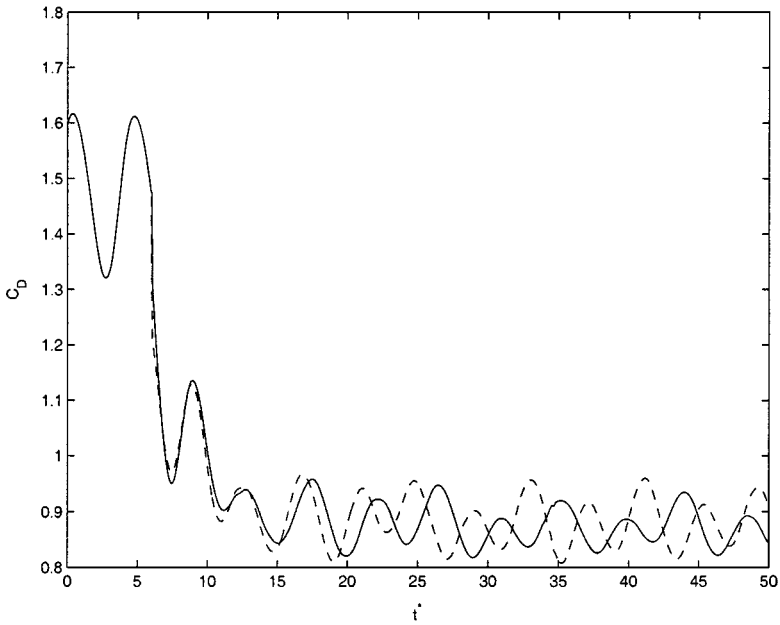

FIG. 21. Validation run, ideal jet actuators: Comparison between the drag coefficient for the case using all the actuators (full line) and the case using only the first four most significant actuators (broken line). Control is switched on at $t^* = 5$ for both cases.

Furthermore, there is no significant correlation between the parameters; this confirms that the relevant feature of drag reduction is that the actuators containing the separation point must perform either antisymmetric or symmetric actions, depending on the action considered, but the actuation strengths do not have to be necessarily correlated.

The validation run performed for the best solution in the population is reported in Fig. 21, which shows a plot of the drag coefficient during the transition from the uncontrolled to the controlled phase. The same plot also reports the drag coefficient resulting from the control performed using only the actuators containing the separation point, and using all the other actuators only to satisfy the zero net mass constraint. In this case the drag reduction obtained is not smaller when fewer actuators are used, an indication of the fact that with ideal jet actuators the actuators containing the separation point play a central role in the drag reduction mechanism.

The time average of the vorticity contours near the cylinder (Fig. 22) shows that the modification in the flow behavior due to this kind of actuation is very similar to the tangential actuation case.

5.2.2. *Optimization of the Most Influential Actuators*

In this case another optimization run was performed using only the four actuators containing the separation point as free parameters, all the other actuators being used uniquely to satisfy the zero net mass constraint. The GA parameters are the same as those in the optimization with four actuators and tangential actuators, i.e., actuators 3, 4, 13, and 14, with all the other actuator parameters set to zero. The GA parameters are fixed to the same value as in the belt actuation optimization with four actuators.

The population clustering in this case is shown in Fig. 23. This clustering is the same as the clustering obtained for these actuators in the optimization using 16 parameters, except that

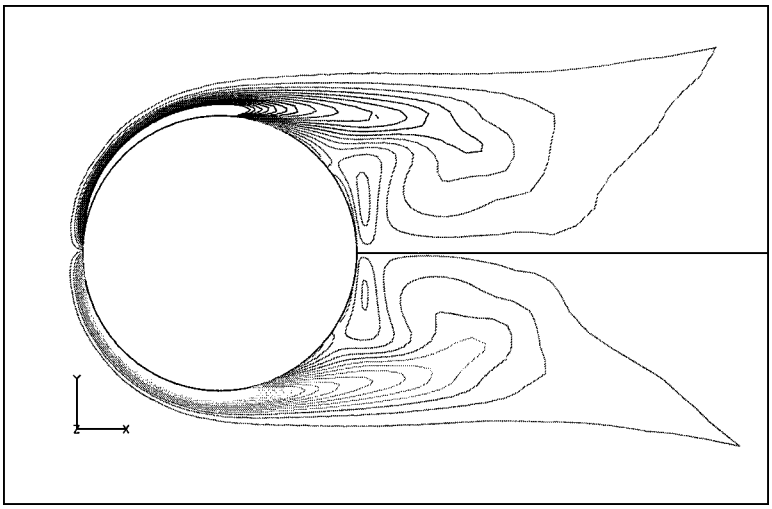

FIG. 22. Ideal jet actuators, only four actuators active: Time-averaged vorticity contours near the cylinder, control switched on.

a more marked sensitivity can be noticed: this implies that when fewer actuators are used, their parameter values become more critical. The validation run showed no improvements with respect to the previous case. This provides us with further evidence that in this case only the actuators containing the separation point are truly important for achieving drag reduction. However, in the case of the tangential belt actuators the reduction is a bit larger than what we observed here.

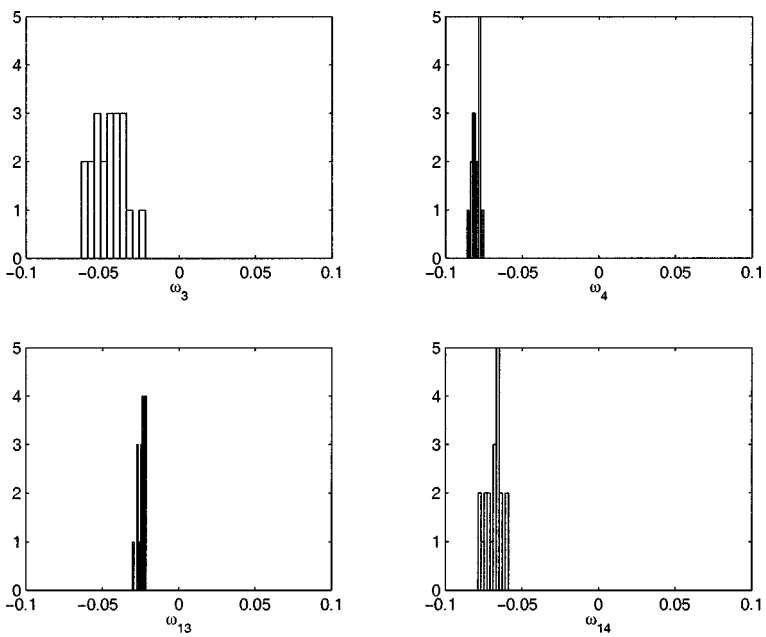

FIG. 23. Ideal jet actuators, optimization run with four actuators: Population clustering.

5.3. Optimization with Penalty Terms for the Control Energy

In the previous cases it was decided to give more importance to some parameters, depending on their sensitivity as signified by the parameter clustering. The assumption behind this criterion is that a low sensitivity (as signified by a nonclustered population) of the cost function for a parameter implies that it has the same influence on the fitness function for every value it assumes in its basin. Therefore, if the value 0 is included in the basin of a low-sensitivity parameter, setting it to 0 will not change the fitness function significantly. This allowed us to reduce the number of degrees of freedom but it provides a rather arbitrary criterion for the parameter selection. In the following sections it will be shown how penalizing the control energy affects the optimal basin, being of great help in the process of selection of suitable solutions.

5.4. Control with Belt Actuators

For the case study considered, since we do not wish to prescribe in advance which actuators will be more important than others, we set $R = \alpha \cdot I^{16}$, where I^{16} is the 16×16 identity matrix, and the scalar $\alpha = 20$, a value chosen in such a way that the two terms in the functional are roughly of the same order of magnitude in the initial stages of the optimization. For this case, the GA parameters are set to the same values as the correspondent case without penalty term. Only the threshold J_T 15 set to 1, a larger value with respect to the other case, to take into account the additional term due to the control energy.

The final parameter distribution for this optimization is shown in Fig. 24. All the parameters are well clustered, and the ones that are not as important for the drag reduction are clustered around 0, as expected.

In Fig. 25 the most significant correlations between the parameters are plotted. Some adjacent actuators are correlated, an indication of the presence of a quite regular velocity pattern. Also, there are correlations between angular velocities of actuators that are near the front of the cylinder and actuators near the rear part, on the wake side. This indicates that the actuators that are near the front actually have an importance in the overall process. Penalizing the control energy allowed the GA to retain only solutions in which a net, nonzero angular speed is necessary for drag reduction, thus allowing us to uncover the optimal velocity profile shape.

The resulting drag reduction for the best individual in the population is the same as that in the first case, meaning that the minimum reached in this case coincides with that reached earlier.

5.5. Control with Mass Transpiration Actuators

Also with the jet actuators the control energy was penalized to have the two terms in the functional be of the same order of magnitude in the initial stages of the optimization. Therefore $R = \alpha \cdot I^{16}$ and $\alpha = 200$ in this case. All the other GA parameters were kept equal to those used in the optimization without penalty terms, and J_T was fixed to 1.5 in this case. The GA converged in about 300 iterations, yielding the population cluster reported in Fig. 26.

The resulting drag reduction performances were the same as those in the case without penalization; therefore they are not reported here. A remarkable difference w.r.t. the

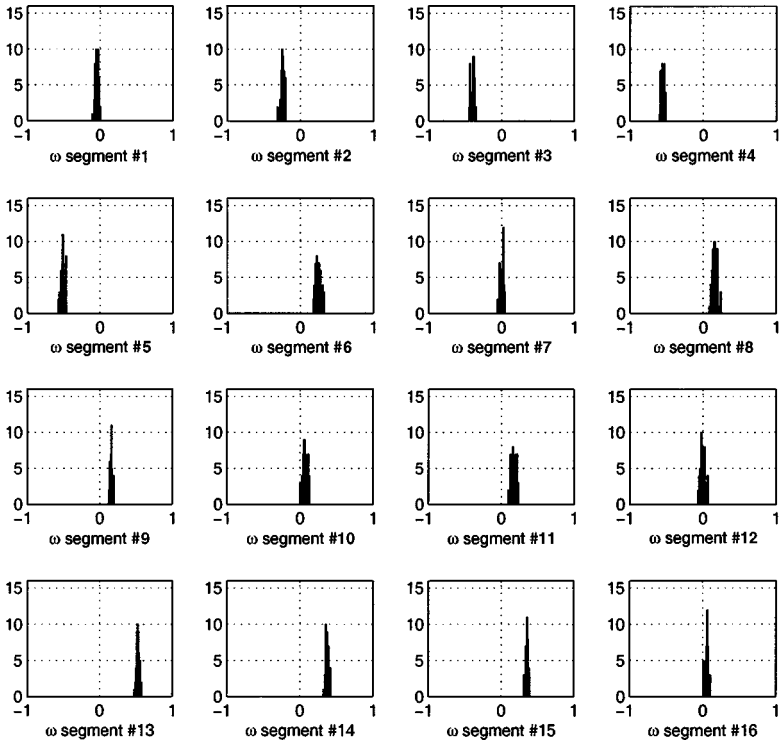

FIG. 24. Optimization with all the actuators, with control energy penalization. Histogram of the final population.

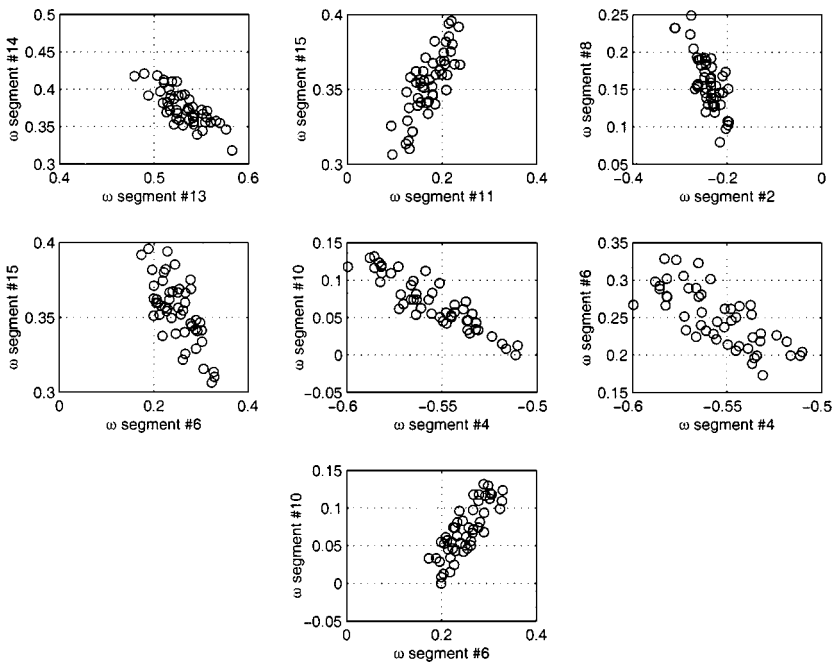

FIG. 25. Optimization with all the actuators, with control energy penalization. Most significant correlations.

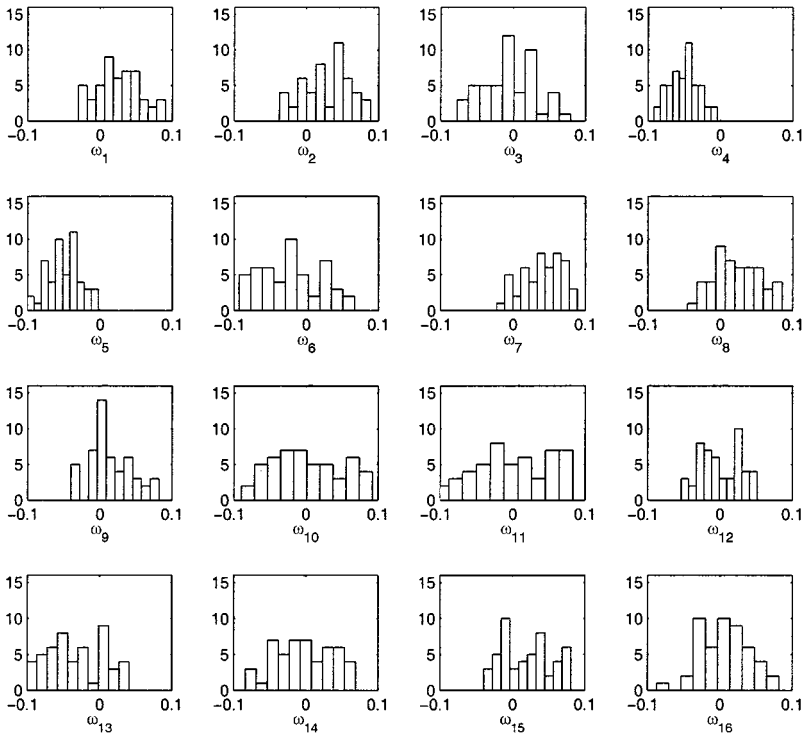

FIG. 26. Jet actuators, optimization with all the actuators, with control energy penalization. Histogram of the final population.

belt actuator optimization is that in this case a control energy penalization equivalent to that used for the belt actuator optimization was used, but the population cluster width did not change significantly. This implies that with jet actuators the parameter sensitivity is much less marked, or in other words the minimum basin is much more shallow in this functional. From a practical viewpoint, it can be inferred that implementation tolerances can be larger in the case of jet actuators, meaning that practical implementation would be easier in this respect for this kind of actuator.

6. TWO-DIMENSIONAL CONTROL FOR THREE-DIMENSIONAL FLOWS

The optimization parameters that were obtained for the two-dimensional simulations are now directly employed for a three-dimensional cylinder with $Re = 500$. It is shown that 2D parameters lead to drag reduction when they are suitably extended for the 3D geometry. A three-dimensional simulation setup with a mesh with $N_r \times N_\theta \times N_z = 160 \times 320 \times 48$ has been used; the cylinder is 5 diameters long, thus ensuring that the simulated flow is three-dimensional [12]. In z direction the tangential velocity has been fixed to be constant and equal to the 2D actuator velocity, to simulate three-dimensional belts.

In Fig. 27 it is possible to see a plot of isosurfaces of positive and negative spanwise vorticity, when the belts are switched off. The separation region is evident from these plots, and it is also possible to see that the vortices are shed from a region near the cylinder. The

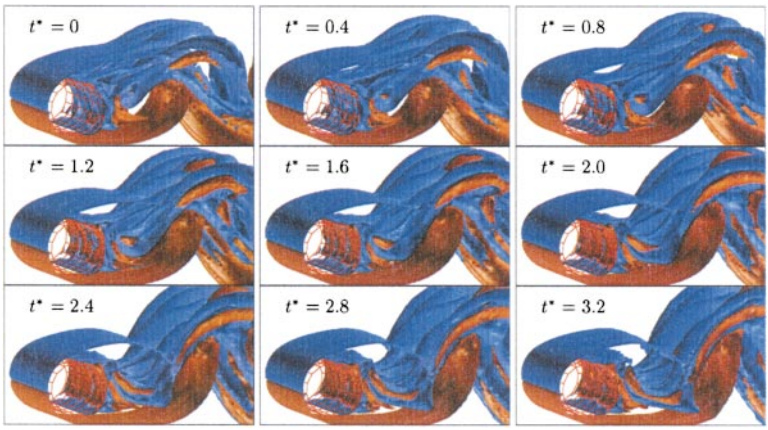

FIG. 27. Uncontrolled shedding of one vortex in the 3D case for the cylinder flow. Blue: Isosurface $\omega_z = 0.1$; red: isosurface $\omega_z = -0.1$.

shedding of one vortex is shown in these plots. In Fig. 28 the transition from uncontrolled shedding to the steady-state controlled shedding is shown; the plots show the same vorticity isosurfaces as before, starting right after the acceleration phase of the belts. Looking at the cylinder surface it is possible to clearly see the separation point moving nearer to the wake region of the cylinder, as well as an elongation of the near wake region. In Fig. 29 the shedding of a vortex in steady state is shown. It is evident that the flow stays much more attached to the cylinder surface, in this case.

The plot of the drag coefficient, corresponding to these vorticity plots, is shown in Fig. 30. After a transition phase, it is possible to see that the drag coefficient settles at a value that is about 50% of the uncontrolled drag coefficient, also in this more realistic simulation. This, however, does not mean that the solution found is the global optimum also in the three-dimensional case: an optimization run should be performed taking into account three-dimensional simulations to be able to draw such a conclusion. This task is the subject

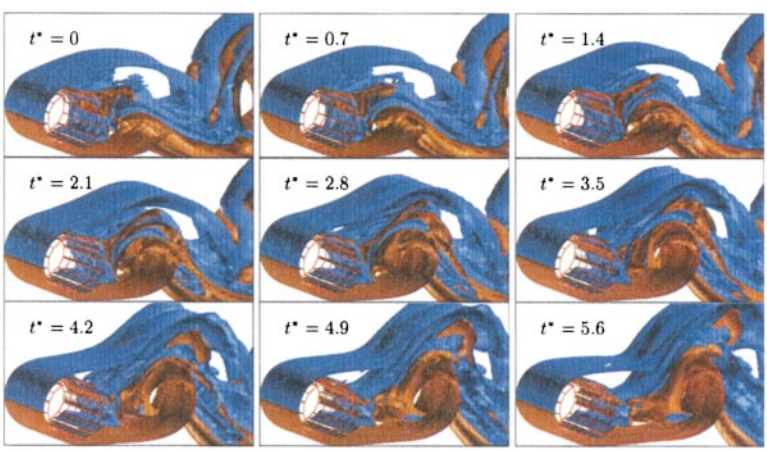

FIG. 28. 3D case cylinder flow, transition from uncontrolled to controlled regime (belt actuators). Blue: Isosurface $\omega_z = 0.1$; red: isosurface $\omega_z = -0.1$.

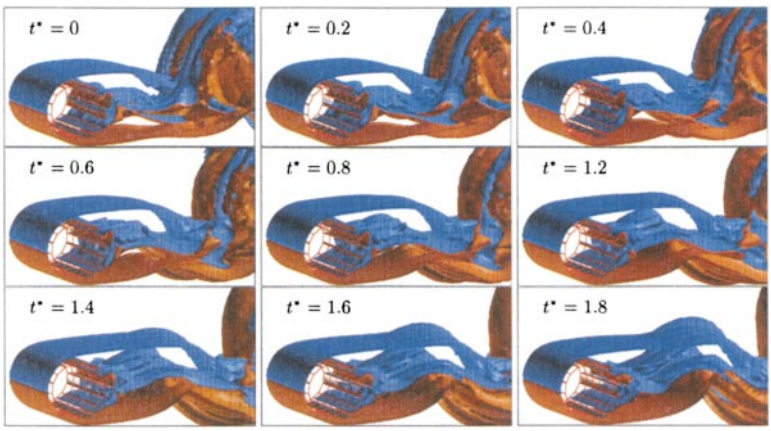

FIG. 29. 3D case cylinder flow, controlled regime (belt actuators). Blue: Isosurface $\omega_z = 0.1$; red: isosurface $\omega_z = -0.1$.

of ongoing work, due to the high computational demand of accurate three-dimensional simulations. An alternative approach using reduced-order models derived from DNS simulations, in conjunction with the proposed GA, also appears to be a promising venue.

However, it is possible to see that the results coming from much less expensive two-dimensional simulations can be extended to three dimensions in a straightforward way, especially when the underlying physical mechanisms are known to be two-dimensional, as in the present case study.

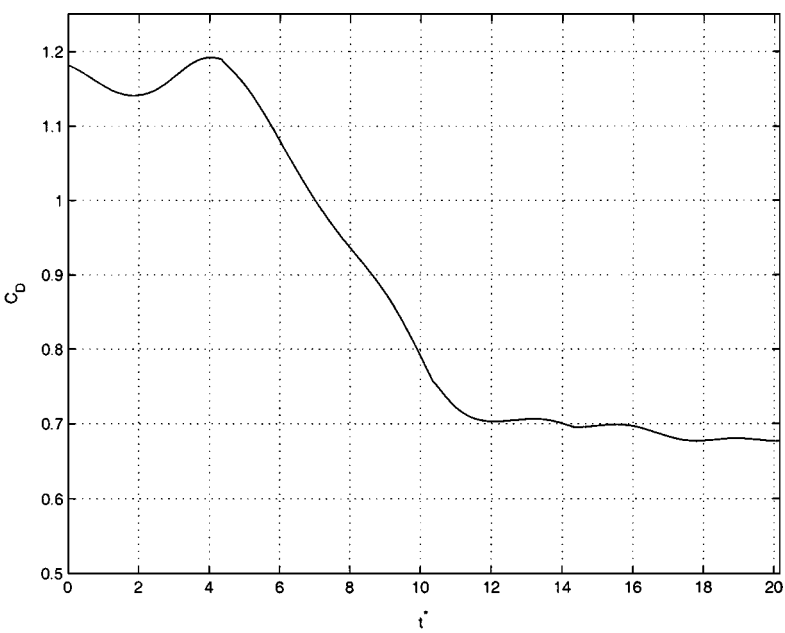

FIG. 30. 3D case cylinder flow, drag coefficient (belt actuators). Transition from the uncontrolled to the controlled regime.

7. CONCLUSIONS

A clustering GA was implemented to study the drag reduction yielded by controlling the velocity field on the surface of a cylinder using idealized actuators. The clustering feature of the algorithm allowed us to examine the parameter correlations and to arrive at optimal surface velocity configurations, yielding a drag reduction of about 50%.

The possibility of using a few strategically placed actuators to obtain a significant drag reduction was explored using the clustering diagnostics of this method. The genetic algorithm provides a systematic way of identifying the significant parameters of the problem pertaining to critical points of the flow such as the separation points. An antisymmetric actuation near the separation points on both sides of the cylinder has been found to be the most important feature of this control system, in the case of belt actuators, while a steady suction in correspondence to the same actuators has been found to have the same effect. The first conclusion that can be drawn is that the GA provided quantitative evidence of what physical understanding would suggest; i.e., to reduce the drag the flow should stay attached to the body surface as long as possible. This "automatic discovery" property of the GA suggests its utilization in cases where scarce physical understanding of the underlying governing mechanism is available. Flow simulations and experiments at high *Re* numbers could be prime targets for this approach. However, the large number of iterations used by GAs and the high computational cost of simulations may be limiting factors. Work is under way to circumvent this difficulty by adapting low-order models to represent the physics of the flow and by accelerating the convergence speed of the GAs exploiting the information that can be gained by unsuccessful trial points during the optimization route.

With regard to the various types of actuation, some conclusion can be drawn by comparing the classes of solutions found for the two different kinds of idealized actuation. This comparison reveals that for mass transpiration the related cost function has a shallower minimum basin. This implies that the tolerances for the mass transpiration actuation strengths can be larger than the tolerances needed for the belt actuators, making them possibly easier to implement.

The results obtained using two-dimensional simulations are shown to be useful for three dimensions when the actuators are suitably extended to the third dimension of the flow. This suggests that optimization in two dimensions followed by a validation of the results in three dimensions is a viable approach to the rapid design of realistic control devices.

ACKNOWLEDGMENT

We express our gratitude to Professor Rajat Mittal, University of Florida, for kindly giving us his cylinder code.

REFERENCES

1. B. D. O. Anderson and J. B. Moore, *Optimal Control* (Prentice Hall, New York, 1994).
2. C. J. Apelt and G. S. West, The effects of wake splitter plates on bluff body flow in the range $10^4 < R < 5 \times 10^4$: Part 2, *J. Fluid Mech.* **71** (1975).
3. D. W. Bechert, W. Hage, and M. Brusek, Drag reduction with the slip wall, *AIAA J.* **34**, No. 5 (1980).
4. B. Choi and H. Choi, Drag reduction with a sliding wall in flow over a circular cylinder, *AIAA J.* **38**, No. 4 (1999).

5. Y. M. Chen, Y. R. Ou, and A. J. Pearlstein, Development of the wake behind a circular cylinder impulsively started into rotatory and rectilinear motion: Intermediate rotation rates, *J. Fluid Mech.* **253** (1993).
6. J. M. Cimbala and S. Garg, Flow in the wake of a freely rotatable cylinder with splitter plate, *AIAA J.* **291** (1991).
7. L. Cortelezzi, Nonlinear feedback control of the wake past a plate with a suction point on the downstream wall, *J. Fluid Mech.* **327** (1996).
8. H. Y. Fan, Inverse design method of diffuser blades by genetic algorithms, *J. Power Energy* **212**, No. 4 (1998).
9. D. W. Fanjoy and W. A. Crossley, Aerodynamic shape design for rotor airfoils via genetic algorithm, *J. Am. Helicopter Soc.* **43**, No. 3 (1998).
10. E. E. Goldberg, *Genetic Algorithms in Search, Optimization and Machine Learning* (Addison–Wesley, Reading, MA, 1989).
11. E. P. Hammond, T. R. Bewley, and P. Moin, Observed mechanisms for turbulence attenuation and enhancement in opposition-controlled wall-bounded flows, *Phys. Fluids* **10** (1998).
12. R. D. Henderson, Nonlinear dynamics and pattern formation in turbulent wake transition, *J. Fluid Mech.* **352** (1997).
13. P. Koumoutsakos, Active control of vortex-wall interactions, *Phys. Fluids* **9** (1997).
14. M. S. Krakov and K. Shiniki, Steady flow past a circular cylinder coated with magnetic fluid: Flow structure, drag reduction and coating deformation, *J. Fluid Mech.* **295** (1995).
15. C. Lee, J. Kim, and H. Choi, Suboptimal control of turbulent channel flow for drag reduction, *J. Fluid Mech.* **358**, 245 (1998).
16. M. Miland, F. Barone, and R. Tagliaferri, A real coded genetic algorithm performing automatic sensitivity analysis (2001). Submitted for publication.
17. R. Mittal, in *Large-Eddy Simulation of Flow Past a Circular Cylinder,* Center for Turbulence Research Annual Research Briefs (1995), p. 107.
18. R. Mittal and S. Balachandar, Effect of three-dimensionality on the lift and drag of nominally two-dimensional cylinders, *Phys. Fluids* **7**, No. 8, 1841 (1995).
19. R. L. Panton, in *Incompressible Flow* (Wiley, New York, 1996), p. 387.
20. O. Shigeru, Y. Yoshihiro, and N. Takashi, Multiobjective genetic algorithm for multidisciplinary design of transonic wing planform, *J. Aircraft* **34**, No. 5, 690 (1997).
21. T. S. Schmit, A. K. Dhingra, F. Landis, and G. Kojasoy, Genetic algorithm optimization technique for compact high density cooler design, *J. Enhanced Heat Transfer* **3**, No. 4, 281 (1996).
22. M. Shumm, E. Berger, and P. A. Monkewitz, Self-excited oscillations in the wake of two-dimensional bluff bodies and their control, *J. Fluid Mech.* **271**, 17 (1994).
23. M. T. Simpson and H. H. Colin, Use of genetic algorithms to optimize vibration actuator placement for active control of harmonic interior noise in a cylinder with floor structure, *Noise Control Eng. J.* **44**, 169 (1996).
24. P. T. Tokumaru and P. E. Dimotakis, Rotary oscillation control of a cylinder wake, *J. Fluid Mech.* **224**, 77 (1991).
25. M. A. Trigg, G. R. Tubby, and A. G. Sheard, Automatic genetic optimization approach to two-dimensional blade profile design for steam turbines, *J. Turbomach. Trans. ASME,* **121**, No. 1, 11 (1999).
26. M. F. Unal and D. Rockwell, On vortex formation from a cylinder. Part 2. Control by splitter plate interference, *J. Fluid Mech.* **190**, 513 (1987).
27. Y. Yajima and O. Sano, Note on the drag reduction of a circular cylinder due to double rows of holes, *Fluid Dyn. Res.* **18**, No. 4, 237 (1996).
28. J. K. Lindsey, *Parametric Statistical Inference* (Clarendon, Oxford, 1996).